156

Весці Нацыянальнай акадэміі навук Беларусі. Серыя фізіка-тэхнічных навук. 2023. Т. 68, №2. С. 156–166
Proceedings of the National Academy of Sciences of Belarus. Physical-technical series, 2023, vol. 68, no. 2, pp. 156–166

Original article

Vladislav S. Volcheck[*], Viktor R. Stempitsky

Belarusian State University of Informatics and Radioelectronics,
6, P. Brovka Str., 220013, Minsk, Republic of Belarus

DEVICE CHARACTERIZATION OF GALLIUM NITRIDE HIGH ELECTRON MOBILITY TRANSISTOR WITH A BORON NITRIDE HEAT-SPREADING ELEMENT

Abstract. A local thermal management solution for high electron mobility transistors based on GaN was developed using a BN layer as a heat-spreading element. The thermally conducting and electrically insulating nature of BN allows it to be placed close to the active area and to be in direct contact with the electrodes and the heat sink, thus introducing an additional heat-escaping route. The numerical simulations of a GaN high electron mobility transistor with the BN heat-spreading element revealed the improvement in the DC, breakdown, small-signal AC and transient characteristics. In case of sapphire substrate, the maximum temperature in the device structure operating at a power density of 3.3 W/mm was reduced by 82.4 °C, while the breakdown voltage at a gate-source voltage of 2 V was increased by 357 V. The cut-off frequency and the maximum oscillation frequency at a gate-source voltage of 6 V and a drain-source voltage of 30 V were enhanced by 1.38 and 1.49 times, respectively. We suppose that the proposed thermal management method can be adapted to other high-power devices.

Keywords: BN, device simulation, GaN, heat dissipation, heat-spreading element, heterostructure field-effect transistor, high electron mobility transistor, power electronics, self-heating, thermal management

Information about the authors: *Vladislav S. Volcheck[*]* – Researcher, Belarusian State University of Informatics and Radioelectronics. E-mail: vlad.volchek@bsuir.by; *Viktor R. Stempitsky* – Cand. Sci. (Engineering), Associate Professor, Vice-Rector for Research and Development, Head of Research and Development Department, Belarusian State University of Informatics and Radioelectronics. E-mail: vstem@bsuir.by

Contribution of the authors: *Vladislav S. Volcheck* – analysis and synthesis of literature, computer simulation, interpretation of the research results, writing and formatting of the text of the manuscript; *Viktor R. Stempitsky* – substantiation of the concept, development of the research methodology, critical revision of the text of the manuscript.

Оригинальная статья

В. С. Волчёк[*], В. Р. Стемпицкий

Белорусский государственный университет информатики и радиоэлектроники,
ул. П. Бровки, 6, 220013, Минск, Республика Беларусь

ЭКСПЛУАТАЦИОННЫЕ ХАРАКТЕРИСТИКИ ТРАНЗИСТОРА С ВЫСОКОЙ ПОДВИЖНОСТЬЮ ЭЛЕКТРОНОВ НА ОСНОВЕ НИТРИДА ГАЛЛИЯ С ТЕПЛООТВОДЯЩИМИ ЭЛЕМЕНТАМИ НА ОСНОВЕ НИТРИДА БОРА

Аннотация. Предлагается метод уменьшения влияния эффекта саморазогрева в транзисторах с высокой подвижностью электронов на основе нитрида галлия, который заключается в использовании слоя нитрида бора в качестве теплоотводящего элемента. Высокая теплопроводность и низкая электрическая проводимость нитрида бора позволяют располагать слой на его основе вблизи активной области и находиться в плотном контакте с электродами и теплопоглощающим элементом, формируя таким образом дополнительный канал для отведения избыточного тепла. Результаты

* Corresponding author / Автор, ответственный за переписку.

Весці Нацыянальнай акадэміі навук Беларусі. Серыя фізіка-тэхнічных навук. 2023. Т. 68, №2. С. 156–166
Proceedings of the National Academy of Sciences of Belarus. Physical-technical series, 2023, vol. 68, no. 2, pp. 156–166

157

численного моделирования транзистора с высокой подвижностью электронов на основе нитрида галлия с теплоотводящим элементом на основе нитрида бора указывают на улучшение электрических, частотных и переходных характеристик, увеличение напряжения пробоя. В случае сапфировой подложки максимальная температура в структуре прибора, работающего на уровне 3,3 Вт/мм, снижается на 82,4 °C, при этом напряжение пробоя, рассчитанное при напряжении затвор-исток 2 В, повышается на 357 В. Граничная частота и максимальная частота генерации, определенные при напряжении затвор-исток 6 В и напряжении сток-исток 30 В, увеличиваются в 1,38 и 1,49 раз, соответственно. Предлагаемое конструктивно-технологическое решение может использоваться и для других мощных приборов.

Ключевые слова: гетероструктурный полевой транзистора, нитрид бора, нитрид галлия, приборное моделирование, рассеяние тепла, саморазогрев, силовая электроника, теплоотводящий элемент, транзистор с высокой подвижностью электронов, управление тепловым режимом

Информация об авторах: *Волчёк Владислав Сергеевич** – научный сотрудник, Белорусский государственный университет информатики и радиоэлектроники. E-mail: vlad.volchek@bsuir.by; *Стемпицкий Виктор Романович* – кандидат технических наук, доцент, проректор по научной работе, начальник научно-исследовательской части, Белорусский государственный университет информатики и радиоэлектроники. E-mail: vstem@bsuir.by

Вклад авторов: *Волчёк Владислав Сергеевич* – анализ и обобщение данных литературы, компьютерное моделирование, интерпретация результатов исследования, написание и оформление текста рукописи; *Стемпицкий Виктор Романович* – обоснование концепции, разработка методологии исследования, критический пересмотр текста рукописи.

Introduction. The advent of power semiconductor devices in the middle of the last century laid a solid foundation for modern power electronics – the branch of electrical engineering that is engaged in the control and conversion of electric power. It has found a broad spectrum of applications, varying in size from a switch-mode power supply in AC adapters, through a variable-frequency drive used in pumping plants, up to a high-voltage DC electric power transmission system. Advancements in power electronics are crucial to unlocking efficient generation, distribution and consumption of electrical energy, since a power conversion system can be found in virtually every electronic component. A major breakthrough that would greatly improve the efficiency by ensuring low switching and conduction losses is expected from the use of novel materials. Since the inception of solid-state electronics, the basic semiconductor for manufacturing power devices has been silicon. However, silicon technology is now failing to meet the requirements of up-to-date industrial applications and, to current opinion, is about to reach its limits [1]. Consequently, there is a continuous trend towards the introduction of next-generation power devices based on wide band gap semiconductors. One of these attractive materials is GaN – a representative of unique group-III nitrides. In 2021, global sales of GaN devices were valued at $1.88 billion and are estimated to expand at a compound annual growth rate of 24.4 % from 2022 to 2030 [2]. Among the benefits offered by GaN transistors, a low on-state resistance, a high breakdown voltage, a high operational switching frequency, along with excellent thermal and radiation stability should be mentioned. Moreover, a definite advantage of GaN is the ability to form different top-quality heterostructures with other group-III nitrides using band-gap engineering. In particular, a two-dimensional electron gas with a sheet concentration of 10^{13} cm^{-2} and a carrier mobility of 2,000 cm^2/(V·s) is usually created in AlGaN/GaN heterostructures [3, 4] due to the spontaneous and piezoelectric components of electrical polarization and to the donor-like surface states acting as the source of electrons [5, 6].

One of the most appealing devices for power electronics is a high electron mobility transistor (HEMT), or a heterostructure field-effect transistor, based on group-III nitrides. It exploits the high in-plane mobility of the two-dimensional electron gas that is generated in the quantum well near the heterojunction. Although GaN HEMTs have significantly advanced in recent times [7, 8], to reveal them as reliable and economically viable devices there are still several fundamental challenges that must be resolved. One such critical problem is the self-heating effect. When a GaN HEMT operates at a high power level, ohmic heating leads to the degradation of the current-voltage characteristics and results in device reliability issues [9]. This phenomenon is observed because of the inherently poor heat dissipation capability of lateral GaN HEMTs.

158

Весці Нацыянальнай акадэміі навук Беларусі. Серыя фізіка-тэхнічных навук. 2023. Т. 68, №2. С. 156–166
Proceedings of the National Academy of Sciences of Belarus. Physical-technical series, 2023, vol. 68, no. 2, pp. 156–166

In order to suppress the self-heating effect, a wide variety of approaches has been proposed to date [10–14]. Most of them, however, act at the package level and fail to remove adequately the excess heat from the active region of the transistor. Therefore, it is necessary to establish a local thermal management method that could be applied at the micrometer scale, or at the device level. Yan *et al.* have demonstrated that the heat dissipation capability of GaN HEMTs can be increased at the micrometer scale by a graphene-graphite heat-spreading element covering the drain contact [15]. Graphene has very exciting prospects for thermal management applications due to its superior in-plane thermal conductivity. Additionally, the heat conduction in graphene is noticeably anisotropic and the out-of-plane thermal conductivity is estimated to be about 0.1 W/(cm·K). This actually may be advantageous, since the heat-spreading element would remove the heat away rather than dissipate it around the hot spot. On the other hand, the extremely good electrical conductance of graphene imposes a limitation on the location of the heat-spreading element, thus requiring an extra photolithography step to pattern graphene and complicating the process flow [16, 17]. Consequently, there is a strong demand for highly thermally conducting but electrically insulating materials. It is well known that diamond falls into this category, but its high temperature and pressure synthesis process is still unacceptably expensive. One of the most promising materials that possess the required properties is BN. Recent measurements showed that the in-plane thermal conductivity of its isotopically near-natural (78 % [11]B, 22 % [10]B) hexagonal form (α-BN) equals to 4.08 W/(cm·K). For the monoisotopic [10]B and [11]BN α-BN crystals, the values of 5.85 and 5.50 W/(cm·K) were obtained, respectively. By analogy with graphene, the heat conduction in hexagonal BN is anisotropic as its out-of-plane thermal conductivity does not exceed a value of 0.033 W/(cm·K) [18]. An efficient local thermal management method using a few-layer α-BN heat-spreading element covering the whole top surface of the device structure was proposed by Lin *et al.* [16].

According to the latest experimental studies, the thermal conductivity of isotopically natural (78.3 % [11]B, 21.7 % [10]B) cubic BN (β-BN) reaches 8.8 W/(cm·K), which is twice as high as the respective value in hexagonal BN. For the isotopically purified [10]B and [11]BN β-BN samples, the values of 16.5 and 16.6 W/(cm·K) were attained, respectively [19]. These results suggest that, at least in terms of thermal conductivity, the cubic form has an advantage over the hexagonal one. In this paper, we show that the performance of GaN HEMTs can be substantially enhanced by the introduction of a heat-spreading element based on β-BN. The thermally conducting and electrically insulating nature of β-BN allows it to be placed close to the conducting channel and to be in direct contact with the electrodes and the heat sink, thus constituting an additional heat-escaping route.

Device Structure. The main object of the research is a normally-off GaN HEMT augmented with a heat-removing system consisting of a β-BN heat-spreading element and a pyrolytic graphite heat sink. A two-dimensional representation of the device structure is shown in Figure 1.

We specifically used AlGaN/AlN/GaN HEMTs with the layered structure that is composed of a 15-nm-thick $Al_{0.14}Ga_{0.86}N$ barrier layer, a 2-nm AlN spacer and a 1.5-µm GaN buffer layer deposited on either a sapphire or a 6H-SiC substrate. Both the barrier layer and the spacer are undoped.
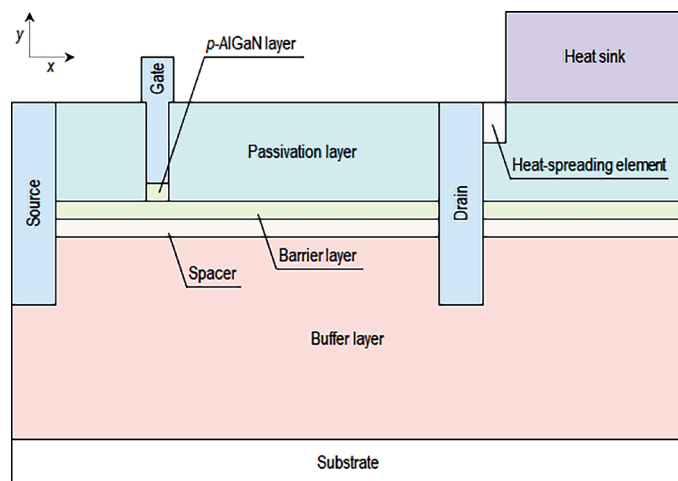
Figure 1. GaN HEMT with a BN heat-spreading element

Весці Нацыянальнай акадэміі навук Беларусі. Серыя фізіка-тэхнічных навук. 2023. Т. 68, №2. С. 156–166
Proceedings of the National Academy of Sciences of Belarus. Physical-technical series, 2023, vol. 68, no. 2, pp. 156–166

159

In the buffer layer, iron-induced deep-level acceptor trap states with an associated energy of 0.7 eV below the conduction band minimum and a uniform concentration of $1 \cdot 10^{18}$ cm^{-3} are introduced to control the drain current in the subthreshold region. Additionally, a 20-nm p-type Al$_{0.14}$Ga$_{0.86}$N layer with an acceptor concentration of $5.3 \cdot 10^{18}$ cm^{-3} is formed beneath the gate to yield a normally-off device [20]. The source, drain and gate electrodes are nominally made of gold and set to be ohmic contacts. Finally, an 0.2-μm SiO$_2$ layer is applied for surface passivation.

The substrate thickness equals to 100 μm. The lengths of the source and drain electrodes are 1 μm, while the lengths of the lower (foot) and higher (head) parts of the T-shaped gate electrode are, respectively, 0.5 and 0.7 μm. The thickness of the gate head is 0.1 μm. The distance from the source to the gate foot is 2 μm and the distance from the gate foot to the drain is 6 μm. The thickness of the heat-spreading element equals to 80 nm. The 20-μm-thick heat sink is located at a distance of 0.5 μm from the drain. The device structure is 1 mm wide.

With the purpose of accurately simulating the temperature distribution, two thermal boundary conditions are imposed, one on the bottom of the substrate and another on the top surface of the heat sink. Both of these regions are sufficiently thick to assume that the temperature at the thermal contacts remains rigid. The thermal boundary resistance (TBR) at the interfaces between the ambient and both the substrate and the heat sink is not taken into consideration. With reference to this, the heat transfer coefficient goes to infinity.

Since the GaN HEMT is grown on a foreign substrate, the self-heating effect is aggravated by the TBR between the substrate and the GaN buffer layer. Although the TBR at the sapphire–GaN interface is negligible owing to the low thermal conductivity of the substrate, this is not the case for the SiC–GaN contact. One approach to model the TBR is to incorporate a very narrow heat isolation layer between the SiC and GaN regions. For a 10-nm-thick layer, its effective thermal conductivity should be set to a value of 0.003 W/(cm·K) [21].

Simulation details. The electrical behavior of semiconductor devices is operated by a mathematical model consisting of a coupled set of fundamental partial differential equations that bind together the electrostatic potential and the carrier concentration. The framework of this model is provided by the Poisson and the carrier continuity equations.

The Poisson equation governs the interaction between the potential and the space charge density:

$$\nabla\left(\varepsilon\varepsilon_0\nabla\varphi\right) = q\left(n - p - N_d^+ + N_a^-\right) - Q, \tag{1}$$

where ε is the relative permittivity, ε_0 is the electric constant, φ is the electrostatic potential, q is the elementary charge, n and p are the electron and hole concentrations, N_d^+ and N_a^- are the ionized donor and acceptor impurity concentrations, Q is the charge density induced by traps and other defects.

The continuity equations describe the way the electron and hole concentrations evolve as a result of transport, generation and recombination processes:

$$\frac{\partial n}{\partial t} = \frac{1}{q}\nabla\overrightarrow{J_n} + G_n - R_n, \tag{2}$$

$$\frac{\partial p}{\partial t} = -\frac{1}{q}\nabla\overrightarrow{J_p} + G_p - R_p, \tag{3}$$

where $\overrightarrow{J_n}$ and $\overrightarrow{J_p}$ are the electron and hole current densities, G_n and G_p are the generation rates for electrons and holes, R_n and R_p are the recombination rates for electrons and holes.

The current density equations, or charge transport models, are often derived by applying various approximations to the Boltzmann transport equation. The simplest transport model is the drift-diffusion model, which has the advantage of not introducing any independent variables in addition to the potential and the carrier concentration:

$$\overrightarrow{J_n} = qD_n\nabla n + q\mu_n n\overrightarrow{E}, \tag{4}$$

$$\overrightarrow{J_p} = qD_p\nabla p - q\mu_p p\overrightarrow{E}, \tag{5}$$

where D_n and D_p are the diffusion coefficients for electrons and holes, μ_n and μ_p are the electron and hole mobilities, $\overrightarrow{E}$ is the electric field related to the potential through the Gauss law:

160

Весці Нацыянальнай акадэміі навук Беларусі. Серыя фізіка-тэхнічных навук. 2023. Т. 68, №2. С. 156–166
Proceedings of the National Academy of Sciences of Belarus. Physical-technical series, 2023, vol. 68, no. 2, pp. 156–166

$$\vec{E} = -\nabla\varphi. \tag{6}$$

Here, it should be noted that the Einstein relationship is tacitly assumed to hold:

$$D_n = V_T \mu_n, \tag{7}$$

$$D_p = V_T \mu_p, \tag{8}$$

where V_T is the thermal voltage:

$$V_T = \frac{\kappa_B T}{q}, \tag{9}$$

where κ_B is the Boltzmann constant, T is the temperature.

The self-consistent solution of the Poisson and the carrier continuity equations must satisfy the boundary conditions specified at the electrodes. Ohmic contacts are implemented as Dirichlet boundary conditions, or first-type boundary conditions, where the potential and the carrier concentration at the surface are fixed. If space charge neutrality is assumed and Maxwell–Boltzmann statistics is applied, the surface electron and hole concentrations are calculated as follows:

$$n_O = \frac{N_d^+ - N_a^- + \sqrt{\left(N_d^+ - N_a^-\right)^2 + 4n_{int}^2}}{2}, \tag{10}$$

$$p_O = \frac{n_{int}^2}{n_O}, \tag{11}$$

where n_{int} is the intrinsic carrier concentration.

In the (Al,Ga)N system, GaN features the narrowest band gap and is therefore used as the reference material in the band alignment. In this case, the surface potential is calculated by

$$\varphi_O = V_T \ln\left(\frac{N_c(GaN) n_O}{n_{int}(GaN) N_c(AlGaN)}\right) + \frac{\chi(GaN)}{q} - \frac{\chi(AlGaN)}{q} - \frac{\varphi_n}{q}, \tag{12}$$

where N_c is the effective density of states for electrons, χ is the electron affinity, φ_n is the electron quasi-Fermi level.

The intrinsic carrier concentration is defined by

$$n_{int} = \sqrt{N_c N_v} \exp\left(-\frac{E_g}{2qV_T}\right), \tag{13}$$

where N_v is the effective density of states for holes, E_g is the band gap.

The temperature dependence of the band gap for AlN, GaN and 6H-SiC is commonly fitted to the empirical Varshni form:

$$E_g(T) = E_g(0 \text{ K}) - \frac{\alpha T^2}{\beta + T}, \tag{14}$$

where α and β are adjustable (Varshni) parameters.

The parameters used in Eq. (14) for AlN, GaN and 6H-SiC are given in Table 1.

For AlGaN, the dependence of the band gap on composition fraction is described by

$$E_g(Al_x Ga_{1-x} N) = E_g(AlN) x + E_g(GaN)(1-x) - C_g x(1-x), \tag{15}$$

where x is the composition fraction, C_g is the bowing parameter, which is recommended to be set to 1.0 eV [22].

Table 1. **Material-dependent parameters for the band gap model**

Material	Parameter		
	E_g (0 K) (eV)	α (meV/K)	β (K)
AlN [22]	6.23	1.799	1462
GaN [22]	3.507	0.909	830
6H-SiC [23]	3.023	0.65	1200

Весці Нацыянальнай акадэміі навук Беларусі. Серыя фізіка-тэхнічных навук. 2023. Т. 68, №2. С. 156–166
Proceedings of the National Academy of Sciences of Belarus. Physical-technical series, 2023, vol. 68, no. 2, pp. 156–166

161

The effective densities of states for electrons and holes, respectively, are defined by

$$N_{\mathrm{c}} = 2\left(\frac{2\pi m_{\mathrm{e}}^{*}\kappa_{\mathrm{B}}T}{h^{2}}\right)^{\frac{3}{2}},\tag{16}$$

$$N_{\mathrm{v}} = 2\left(\frac{2\pi m_{\mathrm{h}}^{*}\kappa_{\mathrm{B}}T}{h^{2}}\right)^{\frac{3}{2}},\tag{17}$$

where m_{e}^{*} and m_{h}^{*} are the density of states effective masses of electrons and holes, h is the Planck constant.

For electrons and holes, we employed the low- and high-field temperature-dependent mobility models specifically developed by Farahmand *et al.* for the (Al,Ga)N material system [24].

In order to simulate the avalanche breakdown characteristics, an impact ionization model was turned on. The electron-hole pair generation rate due to impact ionization is defined by

$$G = \frac{1}{q}\left(\alpha_{n}\left|\vec{J_{n}}\right| + \alpha_{p}\left|\vec{J_{p}}\right|\right),\tag{18}$$

where α_{n} and α_{p} are the ionization coefficients for electrons and holes:

$$\alpha_{n} = a_{n}\exp\left(-\frac{E_{n}}{\left|\vec{E}\right|}\right),\tag{19}$$

$$\alpha_{p} = a_{p}\exp\left(-\frac{E_{p}}{\left|\vec{E}\right|}\right),\tag{20}$$

where a_{n}, a_{p}, E_{n}, E_{p} are adjustable parameters [25].

Modeling of the self-heating effect suggests the addition of a lattice heat flow equation to the coupled system consisting of the Poisson and the carrier continuity equations. In the framework of the thermodynamically rigorous model of lattice heating developed by Wachutka, the heat flow equation, which describes the evolution of the local lattice temperature, has the following form [26]:

$$C_{V}\frac{\partial T_{\mathrm{L}}}{\partial t} = \nabla\left(\kappa\nabla T_{\mathrm{L}}\right) + H,\tag{21}$$

where C_{V} is the volumetric heat capacity, T_{L} is the lattice temperature, κ is the thermal conductivity, H is the heat source per volume unit.

Since ohmic heating is the dominant heat generation process in GaN HEMTs, the other mechanisms are usually neglected [27]. As a result, the heat source per volume unit is reduced to the form

$$H = \left(\vec{J_{n}} + \vec{J_{p}}\right)\vec{E}.\tag{22}$$

It is well known that thermal conductivity and heat capacity are strongly dependent on temperature. This fact must be taken into account, as the operating temperature is very sensitive to the thermal conductivity and heat capacity values in certain regions of the device structure. Otherwise, a significant error will occur.

The temperature dependence of thermal conductivity is often expressed by

$$\kappa(T) = \kappa(300\text{ K})\left(\frac{T}{300}\right)^{\alpha_{\kappa}},\tag{23}$$

where α_{κ} is the temperature dependence coefficient.

For AlGaN, the dependence of the thermal conductivity on composition fraction and temperature is described by [28]

$$\kappa(\mathrm{Al}_{x}\mathrm{Ga}_{1-x}\mathrm{N})(T) = \left[\frac{x}{\kappa(\mathrm{AlN})(T)} + \frac{1-x}{\kappa(\mathrm{GaN})(T)} + C_{\kappa}x(1-x)\right]^{-1},\tag{24}$$

where C_κ is the bowing parameter:

$$C_\kappa = 3.649118 \times 10^{-3} T - 0.221037. \tag{25}$$

We used Eq. (23) for all the unary and binary materials except for gold, for which the thermal conductivity is approximated by a simple linear regression [29]:

$$\kappa(\text{Au})(T) = 3.365 - 6.5 \times 10^{-4} T. \tag{26}$$

The temperature dependence of the volumetric heat capacity of AlN, GaN, 6H-SiC and SiO$_2$ is defined by

$$C_V(T) = \rho C_P (300\ \text{K}) + \rho C_1 \frac{\left(\dfrac{T}{300}\right)^{\alpha_C} - 1}{\left(\dfrac{T}{300}\right)^{\alpha_C} + \dfrac{C_1}{C_P(300\ \text{K})}}, \tag{27}$$

where ρ is the mass density, C_p is the specific heat capacity, C_1 and α_C are adjustable parameters [30].

The dependence of the volumetric heat capacity of Al$_2$O$_3$, gold, β-BN and pyrolytic graphite on temperature is calculated by

$$C_V(T) = a_C + b_C T + c_C T^2 + \frac{d_C}{T^2}, \tag{28}$$

where a_C, b_C, c_C and d_C are adjustable parameters.

When a lattice heat flow equation is solved, at least one thermal boundary condition must be specified. If a thermal contact is implemented as a Robin boundary condition, or a third-type boundary condition, the following expression holds:

$$\alpha(T_\text{L} - T_0) = -\kappa \nabla T_\text{L}, \tag{29}$$

where α is the heat transfer coefficient, T_0 is the ambient temperature, which is assumed to be 300 K.

The material-dependent parameters used in Eqs. (23) and (28) are given in Table 2.

Table 2. **Parameters for the thermal conductivity and volumetric heat capacity models**

Material	Parameter					
	κ (300K) (W/(cm·K))	α_κ	a_C (J/(cm^3·K))	b_C (J/(cm^3·K^2))	c_C (J/(cm^3·K^3))	d_C (J·K/cm^3)
AlN	3.893 [28]	1.277	–	–	–	–
GaN	2.583 [28]	1.031	–	–	–	–
Al$_2$O$_3$	0.387 [31]	1.195	2.839 [33]	0.005	$-2.746 \cdot 10^{-6}$	79 341.95
6H-SiC	3.736 [32]	–1.49	–	–	–	–
SiO$_2$	0.014 [30]	0.33	–	–	–	–
β-BN	8.368 [19]	0.972	1.398 [34]	0.009	$-4.091 \cdot 10^{-6}$	120 197.2
Graphite	19.342 [29]	1.125	–0.944 [35]	0.01	$-5.723 \cdot 10^{-6}$	2661.553
Au	–	–	2.492 [36]	$6.605 \cdot 10^{-5}$	$3.35 \cdot 10^{-7}$	5489.457

Results. The primary subject of the research is a set of the DC, breakdown, small-signal AC and transient characteristics of the GaN HEMTs without and with the heat-spreading element based on cubic BN. In order to investigate the efficiency of our local thermal management solution, we employed a comparative analysis as the main research technique.

The drain current vs. gate-source voltage (curve *1*) and transconductance vs. gate-source voltages (*2*) characteristics of the device structures under study are presented in Figure 2. The drain-source voltage (V_DS) is 0.1 V. As evident from the plot, the GaN HEMT features a normally-off operation with a threshold voltage of 1.98 eV. This value was mainly attained by tuning the acceptor concentration in the *p*-AlGaN layer beneath the gate. Since a low power level is considered, the input characteristics are completely identical regardless of whether a heat-removing system is present or not. The substrate material also makes no difference.

Весці Нацыянальнай акадэміі навук Беларусі. Серыя фізіка-тэхнічных навук. 2023. Т. 68, №2. С. 156–166
Proceedings of the National Academy of Sciences of Belarus. Physical-technical series, 2023, vol. 68, no. 2, pp. 156–166

163
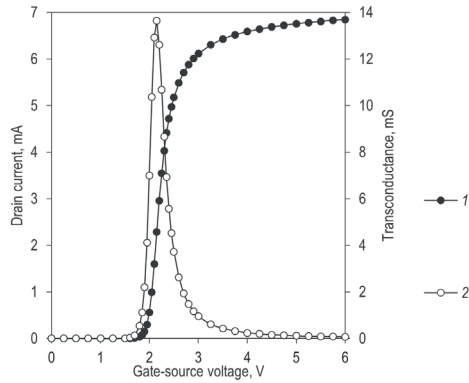
Figure 2. Input DC characteristics at V_{DS} = 0.1 V
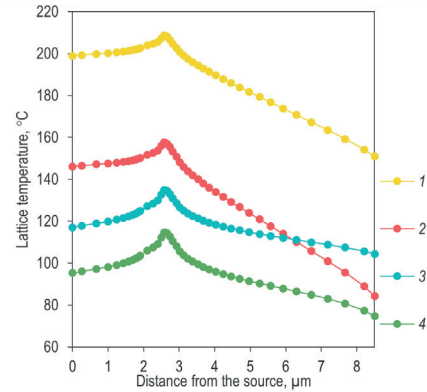
Figure 3. Lattice temperature distribution along
the channel at V_{GS} = 6 V and V_{DS} = 30 V

The efficient operation of the β-BN heat-spreading element is best seen at a high power level. The distribution of the lattice temperature along the conducting channel (along the *x* axis) from the source to drain contacts of the GaN HEMTs without (curves *1*, *3*) and with (curves *2*, *4*) the β-BN layer is shown in Figure 3. The distribution profiles *1* and *2* correspond to sapphire substrate, while *3* and *4* are obtained on 6H-SiC substrate. The gate-source voltage (V_{GS}) is 6 V and the drain-source voltage is 30 V. After the additional heat-escaping route is introduced, the temperature falls dramatically over the whole length of the channel. For instance, at a distance of 0 μm from the source contact, the lattice temperature is decreased from a value of 198.8 to 146.1 °C (ΔT_L = 52.8 °C) when sapphire substrate is used. In case of 6H-SiC substrate, the temperature is decreased from a value of 117.1 to 95.3 °C (ΔT_L = 21.8 °C).

The drain current vs. drain-source voltage (curves *1–4*) and maximum temperature vs. drain-source voltage (curves *5–8*) characteristics of the GaN HEMTs without (curves *1, 3, 5, 7*) and with (curves *2, 4, 6, 8*) the β-BN heat-spreading element are presented in Figure 4. The curves *1, 2, 5* and *6* correspond to sapphire substrate, while curves *3, 4, 7* and *8* are obtained on 6H-SiC substrate. The gate-source voltage is 6 V. Owing to ohmic heating, the current-voltage characteristics show distinct negative-slope regions that indicate a degradation of the electron mobility. However, a reduction in the average temperature within the active area can lead to a partial recovery of the mobility and, consequently, to an improvement of the output power density. After the β-BN layer is formed, the drain current at a drain-source voltage of 30 V is increased by 32.5 %, from a level of 0.123 to 0.163 A, when sapphire substrate is used. The maximum temperature is simultaneously reduced from a value of 208.7 to 157.6 °C (ΔT_L = 51.1 °C). In case of 6H-SiC substrate, the drain current is increased by 16.5 %, from a level of 0.194 to 0.226 A, and the maximum temperature is reduced from a value of 134.8 to 114.7 °C (ΔT_L = 20.1 °C). As the thermal conductivity of 6H-SiC is much higher than that of sapphire, the relative contribution of the on-top heat-removing system to the heat dissipation will be less pronounced.

In Figure 5, the maximum temperature vs. output power density characteristics of the GaN HEMTs on sapphire substrate without (curve *1*) and with (curve *3*) the β-BN heat-spreading element are directly
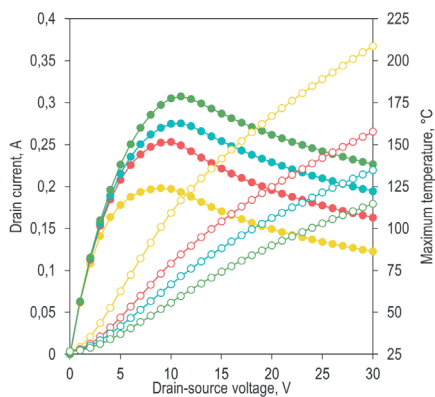
Figure 4. Output DC characteristics at V_{GS} = 6 V
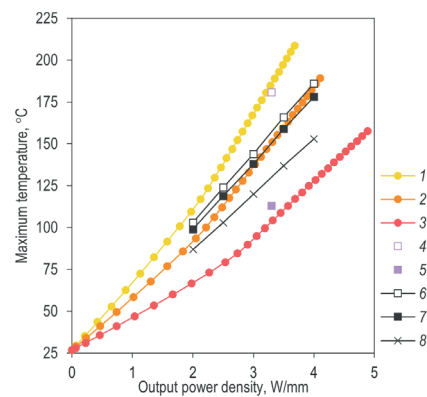
Figure 5. Maximum temperature as a function
of the output power density

164

Весці Нацыянальнай акадэміі навук Беларусі. Серыя фізіка-тэхнічных навук. 2023. Т. 68, № 2. С. 156–166
Proceedings of the National Academy of Sciences of Belarus. Physical-technical series, 2023, vol. 68, no. 2, pp. 156–166

compared with the results published in [15, 16]. In the first paper, the heat dissipation was enhanced by a graphene-graphite quilt covering the drain contact and electrically connected with a graphite heat sink outside of the device structure. At a power density of 3.3 W/mm, the maximum temperature was decreased from a value of 181 °C (data point *4*) to 113 °C (data point *5*) (ΔT_L = 68.0 °C). In the second paper, it was demonstrated that the local thermal management of a GaN HEMT can be substantially improved by a heat-spreading element based on few-layer hexagonal BN stretching over the whole top surface of the device structure. Curve *6* corresponds to the initial device structure. The authors considered two variants differing in the location of the β-BN heat sink that was formed either behind the drain contact (curve *7*) or above the active area (curve *8*). At the same power density, the maximum temperature was decreased from a value of 157.1 to 150.5 °C (ΔT_L = 6.6 °C) and 130.1 °C (ΔT_L = 27.0 °C), respectively. We have recently investigated the DC characteristics of a GaN HEMT with a graphene layer covering not only the drain contact but also the passivation layer [37]. The basic device structure was fully identical to the one used in the current work. The maximum temperature was reduced by 35.3°C, from a value of 185.8 to 150.6 °C, as shown by curve *2*. The simulations results reveal that the β-BN heat-spreading element offers a much higher temperature reduction, to 103.4 °C (ΔT_L = 82.4 °C). It can be explained by the fact that the BN layer partially substitutes the low thermal conductivity SiO_2 passivation layer separating the drain contact from the heat sink.

The heat generation and dissipation processes in GaN HEMTs operated in a pulsed mode are dependent on time, pulse period, duty cycle and other factors. The transient response of the drain current (curves *1, 2*) and the maximum temperature (curves *3, 4*) to a single pulse is given in Figure 6 for the GaN HEMTs on sapphire substrate without (curves *1, 3*) and with (curves *2, 4*) the β-BN heat-spreading element. The off- and on-states are presented by V_{GS} = 0 V and V_{GS} = 6 V, respectively. The drain-source voltage is 30 V. The pulse period and the duty cycle equal to 0.2 ms and 50 %, respectively. As seen from the chart, the device structure containing the β-BN layer is more robust with regard to the self-heating phenomenon. During the on-state time interval, the drain current degrades rapidly to a level of 0.166 A, which is only 37.2 % of an instantaneous value of 0.446 A that would have been obtained if the heat-removing system had been perfect. Simultaneously, the maximum temperature grows sharply and reaches a value of 152.4 °C. In its turn, the performance of the basic device structure is much poorer, as the drain current plummets down to a level of 0.132 A and the maximum temperature rises to a value of 194.9 °C. After being switched off, the transistors gradually cool down and ultimately reach thermal equilibrium with the ambient temperature. The recovery time is determined to be 0.566 and 0.779 ms, respectively.

Figure 7 shows the breakdown characteristics of the GaN HEMTs on sapphire substrate without (curve *1*) and with (curve *2*) the β-BN heat-spreading element. The gate-source voltage is 2 V. In stark contrast to the effect of graphene, the formation of the BN layer leads to an increase in the breakdown voltage, from a value of 821 to 1178 V.

The current gain vs. frequency (curves *1–4*) and unilateral power gain vs. frequency (curves *5–8*) characteristics of the GaN HEMTs without (curves *1, 3, 5, 7*) and with (curves *2, 4, 6, 8*) the β-BN heat-spreading element are presented in Figure 8. The gate-source voltage is 6 V and the drain-source voltage is 30 V. In case of sapphire substrate, the cut-off frequency and the maximum oscillation fre-
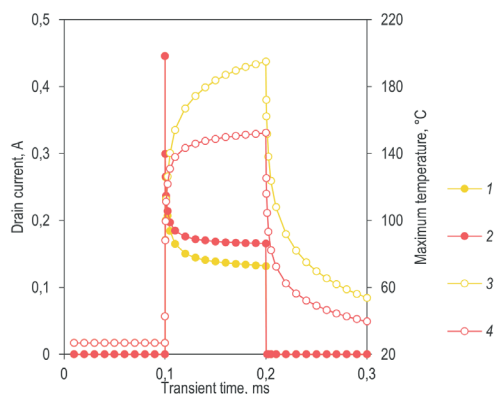
Figure 6. Transient response of the drain current and the maximum temperature to a single pulse
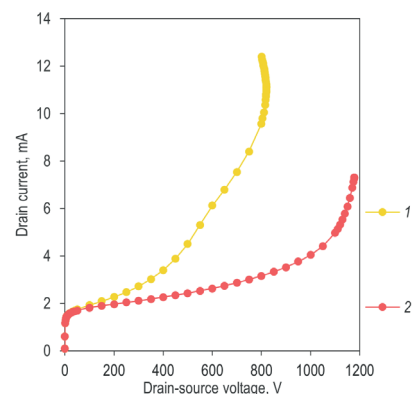
Figure 7. Breakdown characteristics at V_{GS} = 2 V
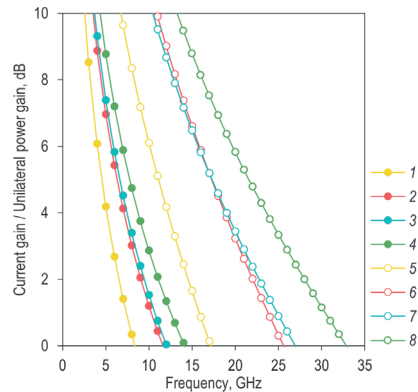
Figure 8. Small-signal AC characteristics at V_{GS} = 6 V and V_{DS} = 30 V

quency are raised by 1.38 times, from a value of 8.4 to 11.6 GHz, and 1.49 times, from a value of 17.2 to 25.6 GHz, respectively. When 6H-SiC substrate is used, the cut-off frequency and the maximum oscillation frequency are enhanced by 1.17 times, from a value of 12.1 to 14.2 GHz, and 1.22 times, from a value of 26.9 to 32.9 GHz, respectively. Nevertheless, these small-signal AC performance quantities are fairly modest in comparison with those provided by the graphene heat-spreading element [37].

Conclusions. In this work, an efficient local thermal management solution using a heat-spreading element based on cubic BN was presented. The thermally conducting and electrically insulating nature of BN allows it to be deposited close to the conducting channel and to be in direct contact with the electrodes and the heat sink, thus constituting an additional heat-escaping route. The numerical simulations of a GaN HEMT with the β-BN heat-spreading element partially substituting the low thermal conductivity SiO_2 passivation layer revealed the improvement in the DC, transient, breakdown and small-signal AC characteristics. In case of sapphire substrate, the maximum temperature in the device structure operating at a power density of 3.3 W/mm was reduced by 82.4 °C.

References

1. Wang Y., Ding Y., Yin Y. Reliability of wide band gap power electronic semiconductor and packaging: A review. *Energies*, 2022, vol. 15, no. 18, art. ID 6670. https://doi.org/10.3390/en15186670

2. *Grand View Research*. Available at: https://www.grandviewresearch.com (accessed 28 October 2022).

3. Gaska R., Yang J. W., Osinsky A., Chen Q., Asif Khan M., Orlov A. O., Snider G. L., Shur M. S. Electron transport in AlGaN-GaN heterostructures grown on 6H-SiC substrates. *Applied Physics Letters*, 1998, vol. 72, no. 6, pp. 707–709. https://doi.org/10.1063/1.120852

4. Gaska R., Shur M. S., Bykhovski A. D., Orlov A. O., Snider G. L. Electron mobility in modulation-doped AlGaN-GaN heterostructures. *Applied Physics Letters*, 1999, vol. 74, no. 2, pp. 287–289. https://doi.org/10.1063/1.123001

5. Smorchkova I. P., Elsass C. R., Ibbetson J. P., Vetury R., Heying B., Fini P., Haus E., DenBaars S. P., Speck J. S., Mishra U. K. Polarization-induced charge and electron mobility in AlGaN/GaN heterostructures grown by plasma-assisted molecular-beam epitaxy. *Journal of Applied Physics*, 1999, vol. 86, no. 8, pp. 4520–4526. https://doi.org/doi/10.1063/1.371396

6. Ibbetson J. P., Fini P. T., Ness K. D., DenBaars S. P., Speck J. S., Mishra U. K. Polarization effects, surface states, and the source of electrons in AlGaN/GaN heterostructure field effect transistors. *Applied Physics Letters*, 2000, vol. 77, no. 2, pp. 250–252. https://doi.org/10.1063/1.126940

7. Tang Y., Shinohara K., Regan D., Corrion A., Brown D., Wong J., Schmitz A., Fung H., Kim S., Micovic M. Ultra-high-speed GaN high-electron-mobility transistors with f_T/f_{max} of 454/444 GHz. *IEEE Electron Device Letters*, 2015, vol. 36, no. 6, pp. 549–551. https://doi.org/10.1109/LED.2015.2421311

8. Chu J., Wang Q., Jiang L., Feng C., Li W., Liu H., Xiao H., Wang X. Room temperature 2DEG mobility above 2350 cm^2/V·s in AlGaN/GaN HEMT grown on GaN substrate. *Journal of Electronic Materials*, 2021, vol. 50, no. 5, pp. 2630–2636. https://doi.org/10.1007/s11664-021-08778-y

9. Trew R. J., Green D. S., Shealy J. B. AlGaN/GaN HFET reliability. *IEEE Microwave Magazine*, 2009, vol. 10, no. 4, pp. 116–127. https://doi.org/10.1109/MMM.2009.932286

10. Alomari M., Dussaigne A., Martin D., Grandjean N., Gaquiere C., Kohn E. AlGaN/GaN HEMT on (111) single crystalline diamond. *Electronics Letters*, 2010, vol. 46, no. 4, pp. 299–301. http://dx.doi.org/10.1049/el.2010.2937

11. Hiroki M., K. Kumakura K., Yamamoto H. Substrate-transfer technique using h-BN for GaN-based high-power transistors. *NTT Technical Review*, 2016, vol. 14, no. 8, pp. 1–6.

12. Feghhi R., Joodaki M. Thermal analysis of microwave GaN-HEMTs in conventional and flip-chip assemblies. *International Journal of RF and Microwave Computer-Aided Engineering*, 2018, vol. 28, no. 8, art. ID e21513. https://doi.org/10.1002/mmce.21513

166

Весці Нацыянальнай акадэміі навук Беларусі. Серыя фізіка-тэхнічных навук. 2023. Т. 68, № 2. С. 156–166
Proceedings of the National Academy of Sciences of Belarus. Physical-technical series, 2023, vol. 68, no. 2, pp. 156–166

13. Pavlidis G., Kim S. H., Abid I., Zegaoui M., Medjdoub F., Graham S. The effects of AlN and copper back side deposition on the performance of etched back GaN/Si HEMTs. *IEEE Electron Device Letters*, 2019, vol. 40, no. 7, pp. 1060–1063. https://doi.org/10.1109/LED.2019.2915984

14. *Fujitsu*. Available at: https://www.fujitsu.com (accessed 19 January 2023).

15. Yan Z., Liu G., Khan J. M., Balandin A. A. Graphene quilts for thermal management of high-power GaN transistors. *Nature Communications*, 2012, vol. 3, no. 1, art. ID 827. https://doi.org/10.1038/ncomms1828

16. Lin Z., Liu C., Chai Y. High thermally conductive and electrically insulating 2D boron nitride nanosheet for efficient heat dissipation of high-power transistors. *2D Materials*, 2016, vol. 3, no. 4, art. ID 041009. https://doi.org/10.1088/2053-1583/3/4/041009

17. Cai Q., Scullion D., Gan W., Falin A., Zhang S., Watanabe K., Taniguchi T., Chen Y., Santos E. J. G., Li L. H. High thermal conductivity of high-quality monolayer boron nitride and its thermal expansion. *Science Advances*, 2019, vol. 5, no. 6, art. ID eaav0129. https://doi.org/10.1126/sciadv.aav0129

18. Yuan C., Li J., Lindsay L., Cherns D., Pomeroy J. W., Liu S., Edgar J. H., Kuball M. Modulating the thermal conductivity in hexagonal boron nitride via controlled boron isotope concentration. *Communications Physics*, 2019, vol. 2, no. 1, art. ID 43. https://doi.org/10.1038/s42005-019-0145-5

19. Chen K., Song B., Ravichandran N. K., Zheng Q., Chen X., Lee H., Sun H., Li S., Gamage G. A., Tian F., Ding Z., Song Q., Rai A., Wu H., Koirala P., Schmidt A. J., Watanabe K., Lv B., Ren Z., Shi L., Cahill D. G., Taniguchi T., Broido D., Chen G. Ultrahigh thermal conductivity in isotope-enriched cubic boron nitride. *Science*, 2020, vol. 367, no. 6477, pp. 555–559. https://doi.org/10.1126/science.aaz6149

20. Uemoto Y., Hikita M., Ueno H., Matsuo H., Ishida H., Yanagihara M., Ueda T., Tanaka T., Ueda D. Gate injection transistor (GIT)–A normally-off AlGaN/GaN power transistor using conductivity modulation. *IEEE Transactions on Electron Devices*, 2007, vol. 54, no. 12, pp. 3393–3399. https://doi.org/10.1109/TED.2007.908601

21. Sarua A., Ji H., Hilton K. P., Wallis D. J., Uren M. J., Martin T., Kuball M. Thermal boundary resistance between GaN and substrate in AlGaN/GaN electronic devices. *IEEE Transactions on Electron Devices*, 2007, vol. 54, no. 12, pp. 3152–3158. https://doi.org/10.1109/TED.2007.908874

22. Vurgaftman I., Meyer J. R., Ram-Mohan L. R. Band parameters for III-V compound semiconductors and their alloys. *Journal of Applied Physics*, 2001, vol. 89, no. 11, pp. 5815–5875. https://doi.org/10.1063/1.1368156

23. Choyke W. J. Optical properties of polytypes of SiC: Interband absorption, and luminescence of nitrogen-exciton complexes. *Materials Research Bulletin*, 1969, vol. 4, pp. S 141–S 152. https://doi.org/10.1016/B978-0-08-006768-1.50018-8

24. Farahmand M., Garetto C., Bellotti E., Brennan K. F., Goano M., Ghillino E., Ghione G., Albrecht J. D., Ruden P. P. Monte Carlo simulation of electron transport in the III-nitride wurtzite phase materials system: Binaries and ternaries. *IEEE Transactions on Electron Devices*, 2001, vol. 48, no. 3, pp. 535–542. https://doi.org/10.1109/16.906448

25. Kunihiro K., Kasahara K., Takahashi Y., Ohno Y. Experimental evaluation of impact ionization coefficients in GaN. *IEEE Electron Device Letters*, 1999, vol. 20, no. 12, pp. 608–610. https://doi.org/10.1109/55.806100

26. Wachutka G. K. Rigorous thermodynamic treatment of heat generation and conduction in semiconductor device modeling. *IEEE Transactions on Computer-Aided Design of Integrated Circuits and Systems*, 1990, vol. 9, no. 11, pp. 1141–1149. https://doi.org/10.1109/43.62751

27. Pomeroy J. W., Uren M. J., Lambert B., Kuball M. Operating channel temperature in GaN HEMTs: DC versus RF accelerated life testing. *Microelectronics Reliability*, 2015, vol. 55, no. 12, pp. 2505–2510. https://doi.org/10.1016/j.microrel.2015.09.025

28. Volcheck V., Hvazdouski D., Baranava M., Stempitsky V. Temperature dependence of the thermal conductivity of wurtzite aluminum nitride, gallium nitride and aluminum-gallium nitride. *Nano-Desing, Tehnology, Computer Simulations: Book of abstracts of XIX International Workshop, Minsk, 28–29 Oct. 2021*. Minsk, BSUIR, 2021, pp. 33–35.

29. Ho C. Y., Powell R. W., Liley P. E. Thermal conductivity of the elements. *Journal of Physical and Chemical Reference Data*, 1972, vol. 1, no. 2, pp. 279–421. https://doi.org/10.1063/1.3253100

30. Palankovski V., Quay R. *Analysis and Simulation of Heterostructure Devices*. Vienna, Springer, 2004. 289 p. https://doi.org/10.1007/978-3-7091-0560-3

31. Dongre B., Carrete J., Mingo N., Madsen G. K. H. Ab initio lattice thermal conductivity of bulk and thin-film α-Al2O3. *MRS Communications*, 2018, vol. 8, no. 3, pp. 1119–1123. https://doi.org/10.1557/mrc.2018.161

32. Burgemeister E. A., von Muench W., Pettenpaul E. Thermal conductivity and electrical properties of 6H silicon carbide. *Journal of Applied Physics*, 1979, vol. 50, no. 9, pp. 5790–5794. https://doi.org/10.1063/1.326720

33. Ditmars D. A., Ishihara S., Chang S. S., Bernstein G., West E. D. Enthalpy and heat-capacity standard reference material: Synthetic sapphire (α-Al_2O_3) from 10 to 2250 K. *Journal of Research of the National Bureau of Standards*, 1982, vol. 87, no. 2, pp. 159–163. https://doi.org/10.6028/jres.087.012

34. Prelas M. A., Gielisse P., Popovici G., Spitsyn B. V., Stacy T. (eds). *Wide Band Gap Electronic Materials*. Dordrecht, Springer, 1995. 531 p. https://doi.org/10.1007/978-94-011-0173-8

35. Butland A. T. D., Maddison R. J. The specific heat of graphite: An evaluation of measurement. *Journal of Nuclear Materials*, 1973, vol. 49, no. 1, pp. 45–56. https://doi.org/10.1016/0022-3115(73)90060-3

36. Takahashi Y., Akiyama H. Heat capacity of gold from 80 to 1000 K. *Thermochimica Acta*, 1986, vol. 109, no. 1, pp. 105–109. https://doi.org/10.1016/0040-6031(86)85012-2

37. Dao D. H., Volcheck V., Stempitsky V., Tran T. T. DC, AC and breakdown simulation of the gallium nitride high electron mobility transistor with a few-layer graphene heat-removal system. *Advanced Technologies for Communications. Proc. 2022 Intern. conf., Hanoi, 20–22 Oct. 2022*. Hanoi, 2022, pp. 121–125. https://doi.org/10.1109/ATC55345.2022.9943047